SUPPORTING INFORMATION

Diketopyrrolopyrrole organic cations as strategy for iodide and lead-free hybrid metal-halide based photoconductors

Théo Forestier,[a] Marcin Kielar,[a] Claudia Wilfinger,[a] Aseem Rajan Kshirsagar,[b] Mikaël Kepenekian,[b] Alexandre Abhervé,[a] and Flavia Pop*[a]*

[a] *Univ Angers, CNRS, MOLTECH-Anjou, SFR MATRIX, F-49000 Angers, France. E-mail: alexandre.abherve@univ-angers.fr, flavia.pop@univ-angers.fr*

[b] *Univ Rennes, ENSCR, CNRS, ISCR – UMR 6226, F-35000 Rennes, France*

Experimental section

Materials and Methods. Solvents and precursors iodomethane (Aldrich), KPF_6 (Aldrich, 99%), $PbCl_2$ (Alfa Aesar, 99.98%), $PbBr_2$ (Fisher Chemical, 98%), PbI_2 (Acros, 99%), $BiBr_3$, hydrobromic acid (HBr, 48% in H_2O, Fluorochem), hydroiodic acid (HI, 57 wt % in H_2O, distilled, stabilized, 99.95%, TCI), were commercially available and used without further purification. 3,6-Di(pyridin-4-yl)-2,5-dihydropyrrolo[3,4-c]pyrrole-1,4-dione (DPP(Py)) was prepared according to literature reports.[1] ^{1}H NMR spectra were recorded with a Bruker AVANCE III 500 (500 MHz). Chemical shifts are given in ppm relative to tetramethylsilane TMS and coupling constants *J* in Hz. Residual non-deuterated solvent was used as an internal standard. The following abbreviations have been used: s, singlet; d, doublet;bs, broaded signal . Mass spectrometry MALDI–TOF MS spectra were recorded on Bruker Biflex-IIITM apparatus, equipped with a 337-nm N2 laser. Powder X-Ray diffraction (PXRD) was performed on a D8 Bruker diffractometer (Cu Kα, λ=1.5418 Å). UV-Vis absorption measurements were performed in reflectance mode using a PerkinElmer LAMBDA 950 spectrophotometer with an integration sphere with a resolution of 2 nm, under room conditions. Photoelectron spectroscopy in air (PESA) measurements were performed on the pressed pellets using a Hitashi AC-5 equipment.

Synthesis of 4,4'-(3,6-dioxo-2,3,5,6-tetrahydropyrrolo[3,4-c]pyrrole-1,4-diyl)bis(1-methylpyridin-1-ium) iodide ((DPP-Py)I_2). 3,6-Di(pyridin-4-yl)-2,5-dihydropyrrolo[3,4-c]pyrrole-1,4-dione (500 mg, 1.7 mmol) was added to acetonitrile (15 mL). Iodomethane (0.4 mL, 6.8 mmol) was added and the mixture was heated at 80°C during 5 days. Two new portions of iodomethane were added during the 5 days of reaction. The cooled reaction mixture was filtered to give the desired product as a purple solid (700 mg, 1.2 mmol, 72%). ^{1}H NMR (500 MHz, DMSO-d6): δ 12.16 (2H, bs, NH), 9.22 (4H, d, J 6.3 Hz, ArH), 8.83 (4H, d, J 6.4 Hz, ArH), 4.38 (6H, s, N-CH_3) ppm (Fig. S1). Elemental analysis calculated for $C_{18}H_{16}N_4O_2I_2$: C, 37.65; H, 2.81; N, 9.46%; found C, 38.00 H, 2.86; N, 9.71%. MS calculated for $C_{18}H_{16}N_4O_2^{2+}$ $[M-2I]^+$ 320.13, found 320.1.

Synthesis of (DPP-Py)(PF_6)$_2$. (DPP-Py)I_2 (1.0 g, 1.74 mmol) was dissolved in 30 ml of acetonitrile and heated to 75°C. KPF_6 (3.2 g, 17.4 mmol) was added as aqueous solution (300 mL) and the mixture was left under stirring overnight 75°C. The solvent was evaporated and the obtained solid was washed with ethanol to remove the excess of KPF_6. The solid was further washed with acetone and dried under vacuum to afford pure desired sample as black solid (430 mg, 40%). Elemental analysis calculated for $C_{18}H_{16}F_{12}N_4O_2P_2$: C, 35.43; H, 2.64; N, 9.18%; found C, 35.66 H, 2.69; N, 9.11%.

Synthesis of (DPP-Py)Pb_2Cl_6. (DPP-Py)PF_6 (93 mg, 0.15 mmol) and $PbCl_2$ (56 mg, 0.2 mmol) were dissolved in HCl (10 mL) and the mixture was stirred at 60°C for 1h. The solution was filtered and cooled to RT. Slow diffusion of EtOAc for three days afforded black needle-like single crystals suitable for X-ray diffraction analysis. The sample was filtered and washed with EtOAc. The purity was confirmed by PXRD.

---

[1] Ftouni, H.; Bolze F.; Nicoud, J. Water-soluble diketopyrrolopyrrole derivatives for two-photon excited fluorescence microscopy. *Dyes Pigm.* **2013**, *97*, 77-83.

Synthesis of (DPP-Py)Pb_2Br_6. The compound was obtained in a similar manner to (DPP-Py)Pb_2Cl_6 starting from $PbBr_2$ (73 mg, 0.2 mmol) and HBr (10 mL). Black needle-like single crystals suitable for X-ray diffraction analysis were obtained. The purity was confirmed by PXRD.

Synthesis of $(H_{13}O_6)$(DPP-Py)$_2Pb_2Br_9$. The compound was obtained in a similar manner to (DPP-Py)Pb_2Br_6 starting from (DPP-Py)I_2 (15 mg, 0.026 mmol) and $PbBr_2$ (9.6 mg, 0.026 mmol). Black platelet-like single crystals suitable for X-ray diffraction analysis were obtained.

Synthesis of (H_9O_4)(DPP-Py)$_2Pb_2Br_9$. The compound was obtained in a similar manner to (DPP-Py)Pb_2Br_6 starting from (DPP-Py)I_2 (17 mg, 0.03 mmol) and $PbBr_2$ (5.5 mg, 0.015 mmol). Brown needle-like single crystals suitable for X-ray diffraction analysis were obtained.

Synthesis of (DPP-Py)Pb_2I_6·$(DMF)_2$ and (DPP-Py)Pb_2I_6·$(DMSO)_2$. (DPP-Py)PF_6 (93 mg, 0.15 mmol) and PbI_2 (92 mg, 0.2 mmol) were dissolved in DMF (10 mL). Few drops of HI were added and the mixture was stirred at 60°C for 1h. The precipitate was filtered and rinsed with EtOAc. Slow diffusion of EtOAc into the filtrate for two days afforded black needle-like single crystals suitable for X-ray diffraction analysis. Both precipitate and single crystals correspond to (DPP-Py)Pb_2I_6·$(DMF)_2$ as confirmed by PXRD. A part of the precipitate was further dissolved in DMSO (10 mL) at 70°C and stirred for 1h. Slow diffusion of diethyl ether in the solution afforded black platelet-like single crystals of (DPP-Py)Pb_2I_6·$(DMSO)_2$.

Synthesis of (DPP-Py)$BiBr_5$. The compound was obtained in a similar manner to (DPP-Py)Pb_2Br_6 starting from $BiBr_3$ (90 mg, 0.2 mmol). Black needle-like single crystals suitable for X-ray diffraction analysis were obtained. The purity was confirmed by PXRD.

X-ray Crystallography. Single crystals of the compounds were mounted on glass fibre loops using a viscous hydrocarbon oil to coat the crystal and then transferred directly to the cold nitrogen stream. Data collection were performed at 200 K on an Agilent Supernova with Cu-K_α (λ = 1.54184 Å). The structures were solved by dual-space algorithm and refined against all F^2 values with the SHELX package[2] using the WinGX graphical user interface. All non-hydrogen atoms were refined anisotropically. All hydrogen atoms were placed in calculated positions and refined isotropically with a riding model. A summary of the crystallographic data and the structure refinement is given in Tables S1-S2. CCDC 2494685-2494692 contain the supplementary crystallographic data for the paper.

Device fabrication and characterization. Gold electrodes were evaporated using a Plassys ME-300 evaporator at the rate of 0.4 nm s^{-1} while maintaining a vacuum pressure of 8.10^{-7} mbar. A deep-blue high-power LED from *Intelligent LED Solutions* (ILS ILH-OW04-DEBL-SC211-WIR200) calibrated with an IR + Visible Light Si photodiode (BPX61, *ams OSRAM*) was used for photoconductivity measurements. The maximum irradiance was 1 mW mm^{-2}. I-V characteristics were performed using a Keithley 2636B dual-channel source-measure unit (*Tektronix*) associated with LabVIEW scripts (National Instruments). All measurements were

[2] G. M. Sheldrick, *Programs for the Refinement of Crystal Structures*; University of Göttingen: Göttingen, Germany, 1996.

performed in air and at room temperature. Increase (in %) of current response upon irradiation was calculated as follows: Delta Current = I(photocurrent) – I(dark) / I(dark).

Table S1 Crystallographic Data for (DPP-Py)I_2, (DPP-Py)Pb_2I_6·$(DMF)_2$, (DPP-Py)Pb_2I_6·$(DMSO)_2$ and (DPP-Py)$BiBr_5$.

	(DPP-Py)I_2	(DPP-Py)Pb_2I_6 ·$(DMF)_2$	(DPP-Py)Pb_2I_6 ·$(DMSO)_2$	(DPP-Py)$BiBr_5$
Empirical formula	$C_{20}H_{15}N_4O_2I_2$	$C_{24}H_{30}N_6O_4I_6Pb_2$	$C_{22}H_{28}N_4O_4S_2I_6Pb_2$	$C_{18}H_{16}N_4O_2Br_5Bi$
Fw	287.07	1642.32	1652.38	928.88
Crystal color	Red	Black	Black	Black
Crystal size (mm^3)	0.17*0.04*0.03	0.29*0.04*0.04	0.19*0.09*0.06	0.09*0.03*0.02
Temperature (K)	200	200	200	230
Wavelength (Å)	1.54184	1.54184	1.54184	1.54184
Crystal system, Z	Monoclinic, 4	Monoclinic, 2	Triclinic, 1	Monoclinic, 4
Space group	$P2_1/c$	$P2_1/n$	P-1	$C2/c$
a (Å)	4.9281(2)	9.7310(5)	8.1967(4)	13.1538(10)
b (Å)	10.3820(4)	8.2091(4)	9.1368(4)	20.3764(13)
c (Å)	18.3674(7)	24.3633(18)	13.2153(6)	9.0431(7)
α (°)	90	90	102.695(4)	90
β (°)	92.341(3)	91.423(5)	95.518(4)	100.093(7)
γ (°)	90	90	93.869(4)	90
V ($Å^3$)	938.96(6)	1945.6(2)	957.04(8)	2386.3(3)
ρ_{calc} ($g.cm^{-3}$)	2.031	2.803	2.867	2.586
μ(CuKα) (mm^{-1})	26.482	54.300	56.178	24.512
θ range (°)	4.819–71.678	3.630–72.414	3.451–72.169	4.045–72.147
Data collected	4000	7788	6755	4990
Data unique	1778	3704	3603	2291
Data observed	1726	2821	3344	1850
R(int)	0.0238	0.0952	0.0683	0.0651
Nb of parameters / restraints	119/0	190/0	183/0	138/0
$R1(F)$,[a] $I > 2\sigma(I)$	0.0418	0.0963	0.0789	0.0535
$wR2(F^2)$,[b] all data	0.1033	0.2943	0.2101	0.1356
$S(F^2)$,[c] all data	1.319	1.069	1.049	1.045

[a] $R1(F) = \Sigma||F_0|-|F_C||/\Sigma|F_0|$; [b] $wR2(F^2) = [\Sigma w(F_0^2-F_C^2)^2/\Sigma wF_0^4]^{1/2}$; [c] $S(F^2) = [\Sigma w(F_0^2-F_C^2)^2/(n+r-p)]^{1/2}$.

Table S2 Crystallographic Data for (DPP-Py)Pb_2Cl_6, (DPP-Py)Pb_2Br_6, ($H_{13}O_6$)(DPP-Py)$_2Pb_2Br_9$ and (H_9O_4)(DPP-Py)$_2Pb_2Br_9$.

	(DPP-Py)Pb_2Cl_6	(DPP-Py)Pb_2Br_6	($H_{13}O_6$)(DPP-Py)$_2$ Pb_2Br_9	(H_9O_4)(DPP-Py)$_2$ Pb_2Br_9
Empirical formula	$C_{18}H_{16}N_4O_2Cl_6Pb_2$	$C_{18}H_{16}N_4O_2Br_6Pb_2$	$C_{36}H_{45}N_8O_{10}Br_9Pb_2$	$C_{36}H_{41}N_8O_8Br_9Pb_2$
Fw	947.43	1214.19	1883.37	1847.34
Crystal color	Black	Black	Black	Brown
Crystal size (mm^3)	0.21*0.05*0.04	0.45*0.43*0.15	0.14*0.09*0.06	0.18*0.07*0.05
Temperature (K)	200	180	200	200
Wavelength (Å)	1.54184	1.54184	1.54184	1.54184
Crystal system, Z	Monoclinic, 2	Monoclinic, 2	Triclinic, 1	Monoclinic, 2
Space group	$P2_1/n$	$P2_1/c$	P-1	$I2/m$
a (Å)	4.0195(2)	4.1449(2)	9.9282(2)	18.4120(7)
b (Å)	17.1565(7)	17.5077(5)	10.0715(3)	6.3623(3)
c (Å)	16.7619(6)	17.0660(5)	13.1792(3)	22.4728(8)
α (°)	90	90	78.571(2)	90
β (°)	96.904(4)	94.779(3)	89.853(2)	108.424(4)
γ (°)	90	90	85.428(2)	90
V ($Å^3$)	1147.53(9)	1234.13(8)	1287.45(6)	2497.59(18)
ρ_{calc} ($g.cm^{-3}$)	2.742	3.267	2.429	2.456
μ(CuKα) (mm^{-1})	34.852	37.813	21.243	21.851
θ range (°)	3.700–76.253	3.623–76.031	3.422–76.284	2.717–76.231
Data collected	5136	5201	21357	6290
Data unique	2310	2499	5203	2774
Data observed	2127	2354	5132	2587
R(int)	0.0447	0.0379	0.0597	0.0392
Nb of parameters / restraints	145/0	145/0	295/0	191/6
$R1(F)$,[a] $I > 2\sigma(I)$	0.0481	0.0445	0.0429	0.0709
$wR2(F^2)$,[b] all data	0.1310	0.1172	0.1150	0.2084
$S(F^2)$,[c] all data	1.069	1.083	1.036	1.055

[a]$R1(F) = \Sigma||F_0|-|F_C||/\Sigma|F_0|$; [b]$wR2(F^2) = [\Sigma w(F_0^2-F_C^2)^2/\Sigma wF_0^4]^{1/2}$; [c]$S(F^2) = [\Sigma w(F_0^2-F_C^2)^2/(n+r-p)]^{1/2}$.

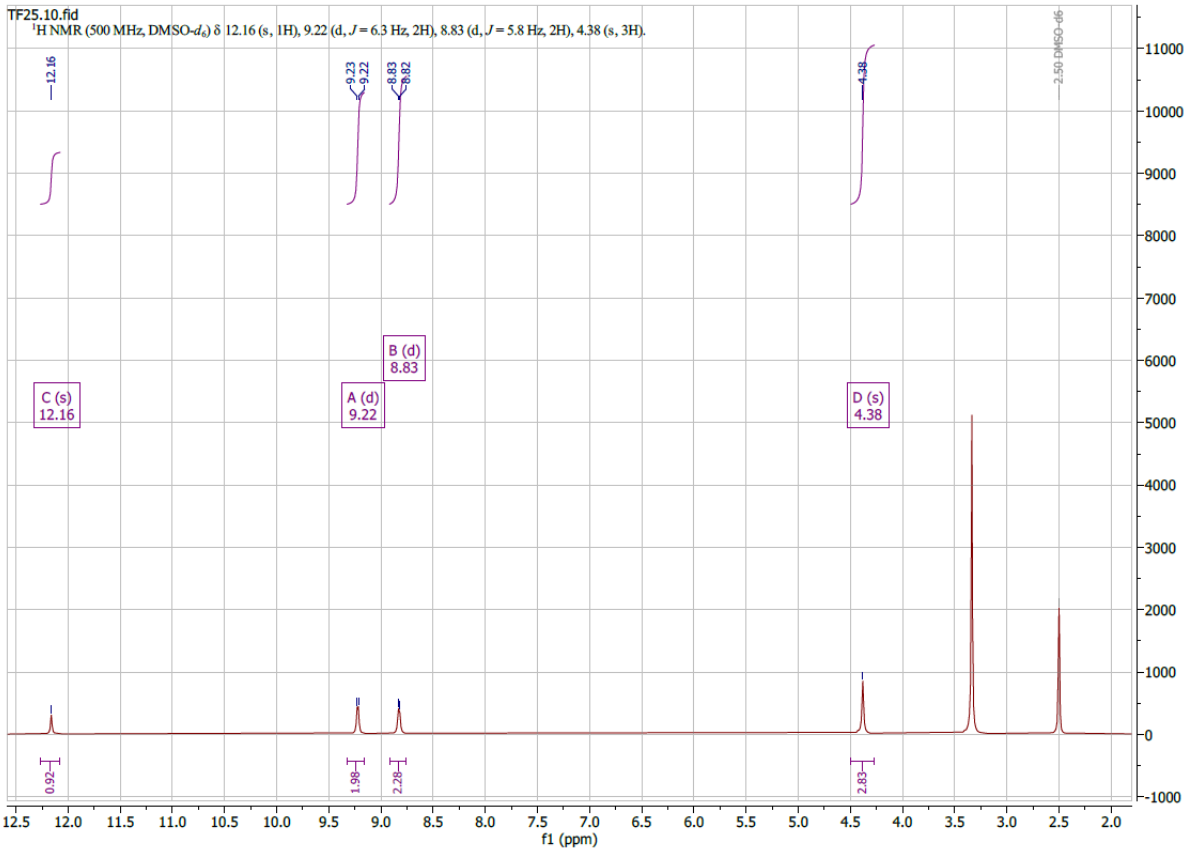

Fig. S1 ^{1}H NMR spectrum of (DPP-Py)I_2.

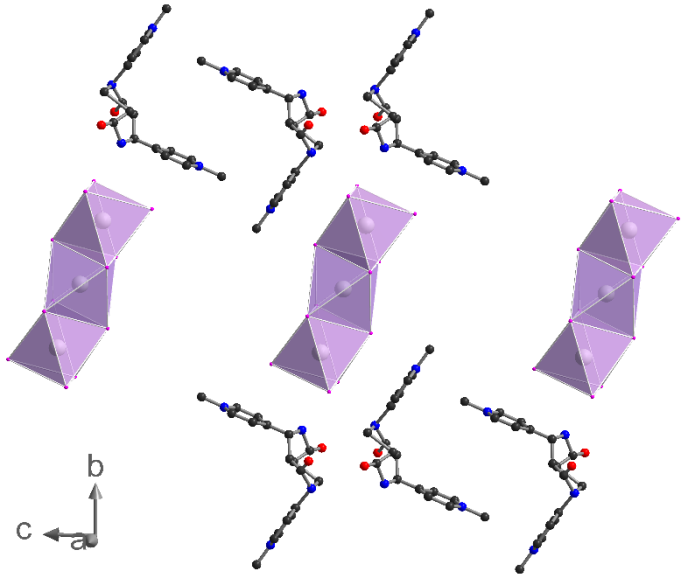

Fig. S2 Crystal structure of (H_4DPP-Py)Pb_3I_{12}.

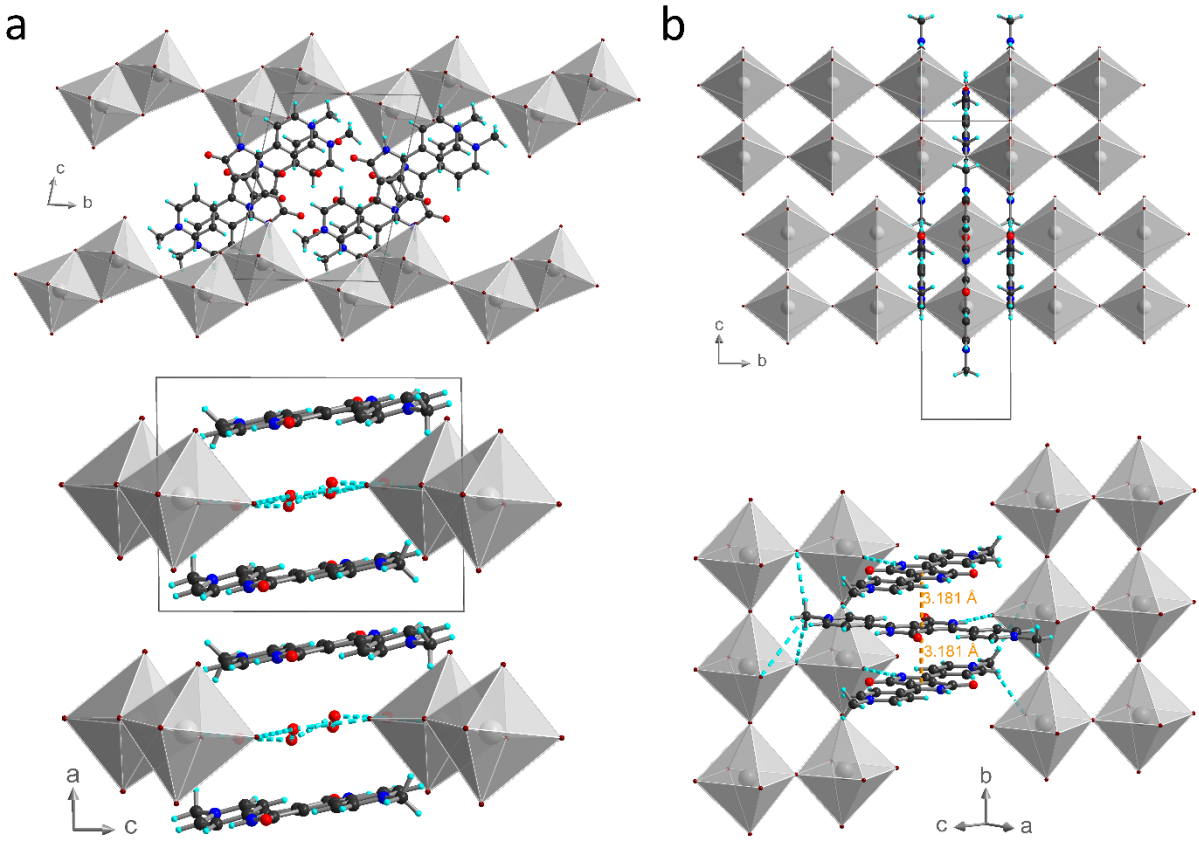

Fig. S3 Crystal structures of (a) $(H_{13}O_6)(DPP\text{-}Py)_2Pb_2Br_9$ and (b) $(H_9O_4)(DPP\text{-}Py)_2Pb_2Br_9$. Color code: C (black), H (cyan), N (blue), O (red), $PbBr_6$ (grey octahedra), hydrogen bonding interactions (cyan dashed lines).

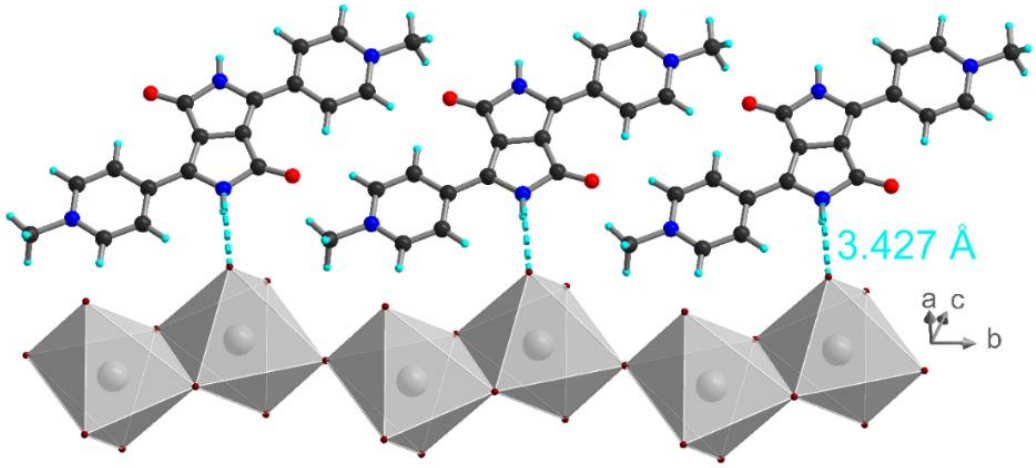

Fig. S4 Intermolecular interactions in $(H_{13}O_6)(DPP\text{-}Py)_2Pb_2Br_9$. Color code: C (black), H (cyan), N (blue), O (red), $PbBr_6$ (grey octahedra), N-H···Br interactions (cyan dashed lines).

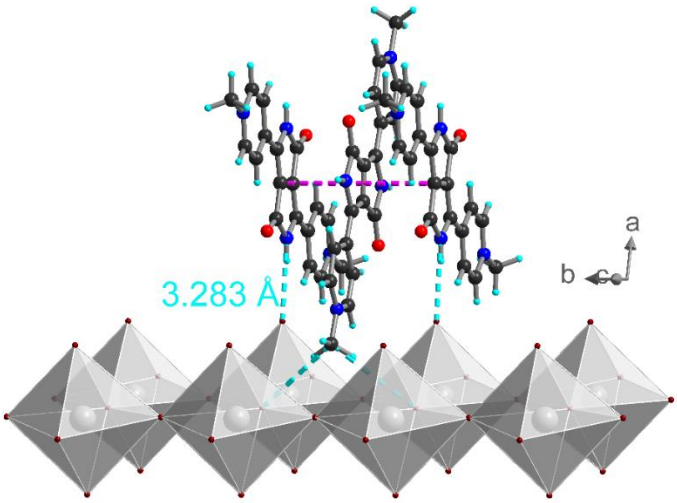

Fig. S5 Intermolecular interactions in $(H_9O_4)(DPP\text{-}Py)_2Pb_2Br_9$. Color code: C (black), H (cyan), N (blue), O (red), $PbBr_6$ (grey octahedra), N-H···Br interactions (cyan dashed lines), π-π stacking (pink dashed lines).

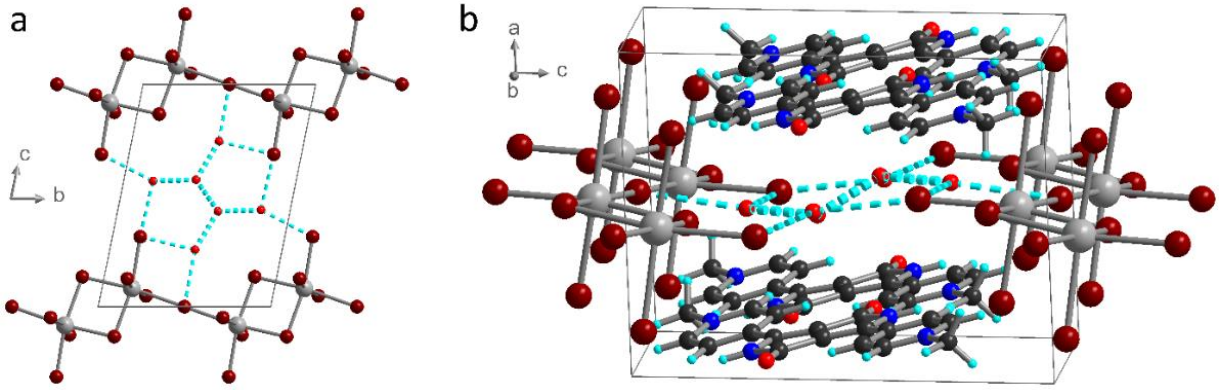

Fig. S6 Hydronium cluster in $(H_{13}O_6)(DPP\text{-}Py)_2Pb_2Br_9$. Color code: C (black), H (cyan), N (blue), O (red), Br (brown), Pb (grey), hydrogen bonding interactions (cyan dashed lines).

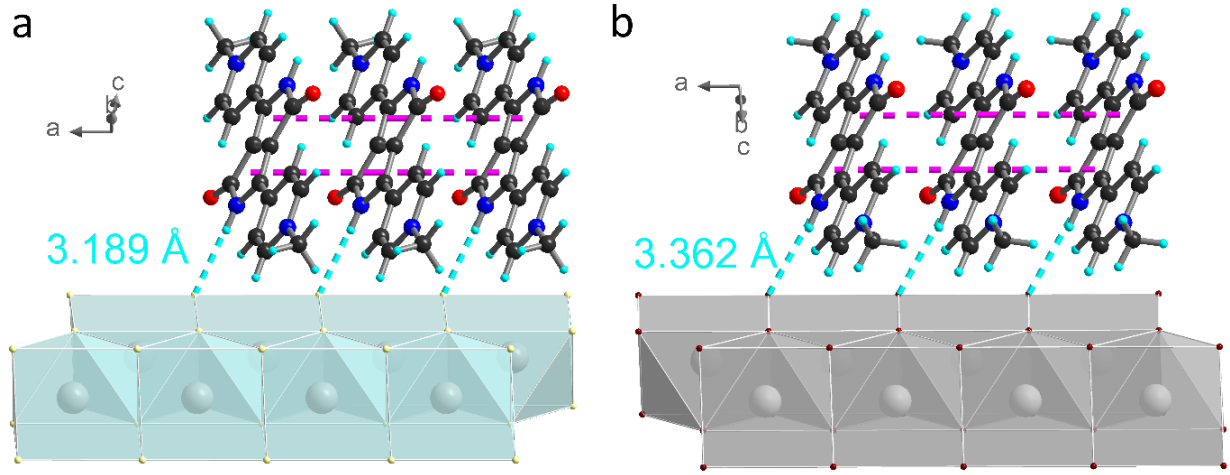

Fig. S7 Intermolecular interactions in (a) $(DPP\text{-}Py)Pb_2Cl_6$ and (b) $(DPP\text{-}Py)Pb_2Br_6$. Color code: C (black), H (cyan), N (blue), O (red), $PbCl_7$ (turquoise octahedra), $PbBr_7$ (grey octahedra), N-H···X interactions (cyan dashed lines), π-π stacking (pink dashed lines).

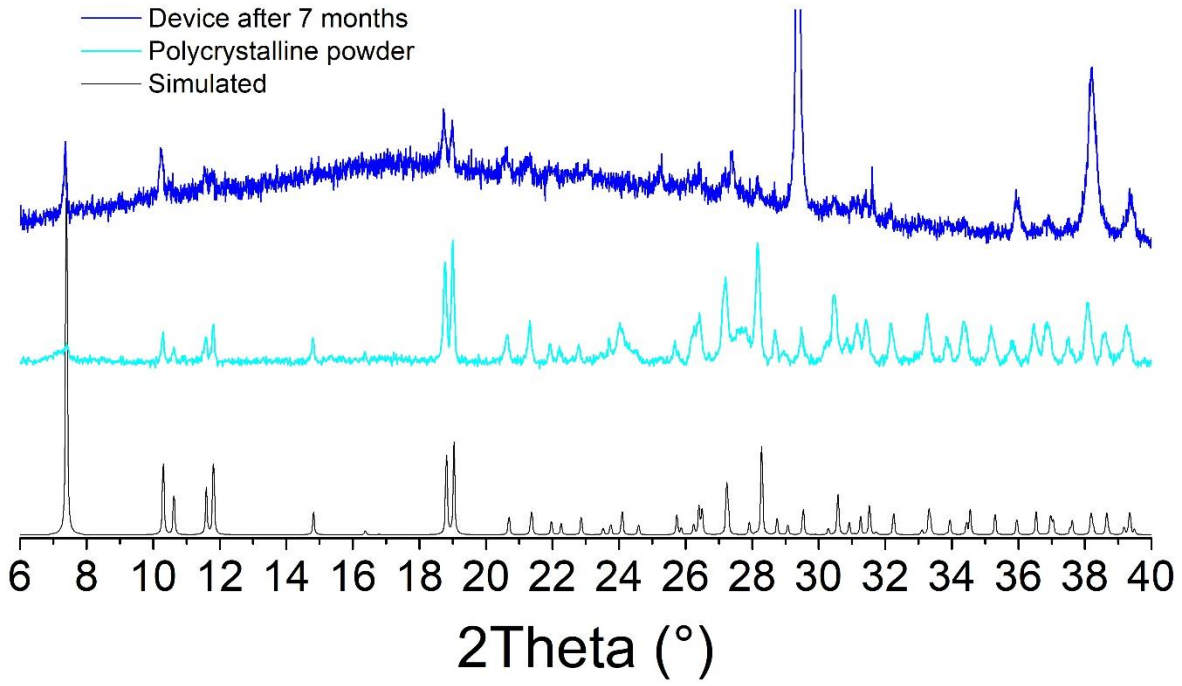

Fig. S8 Simulated and experimental powder X-ray diffraction pattern for (DPP-Py)Pb_2Cl_6.

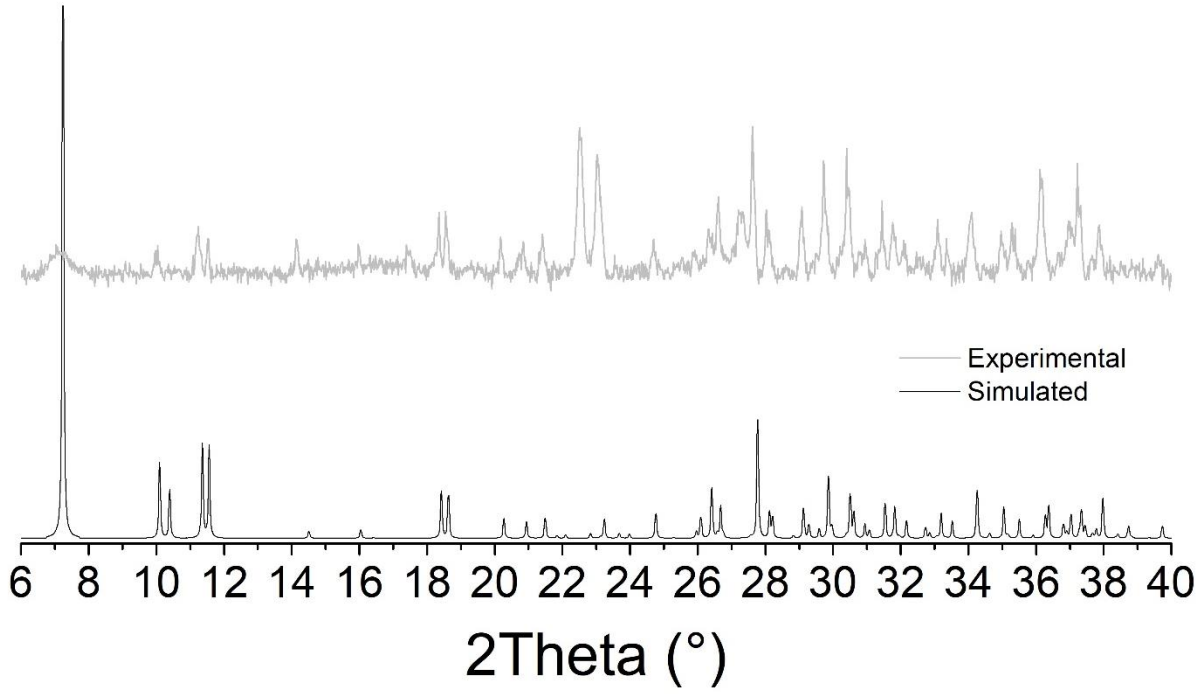

Fig. S9 Simulated and experimental powder X-ray diffraction pattern for (DPP-Py)Pb_2Br_6.

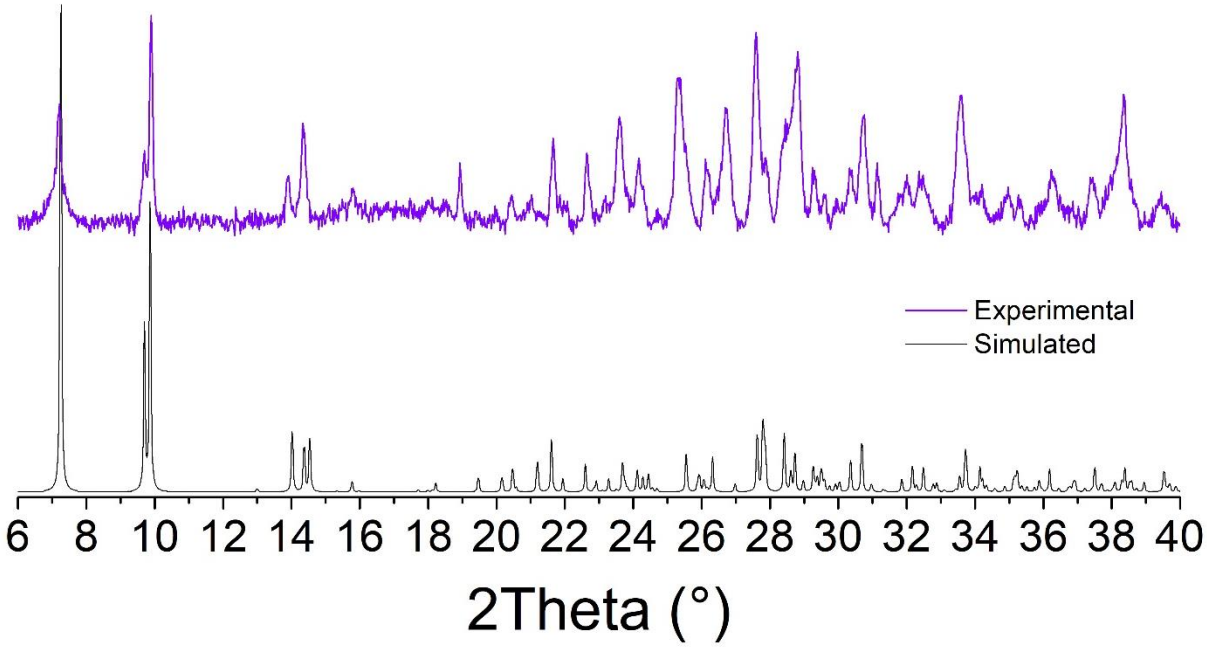

Fig. S10 Simulated and experimental powder X-ray diffraction pattern for (DPP-Py)Pb_2I_6·DMF.

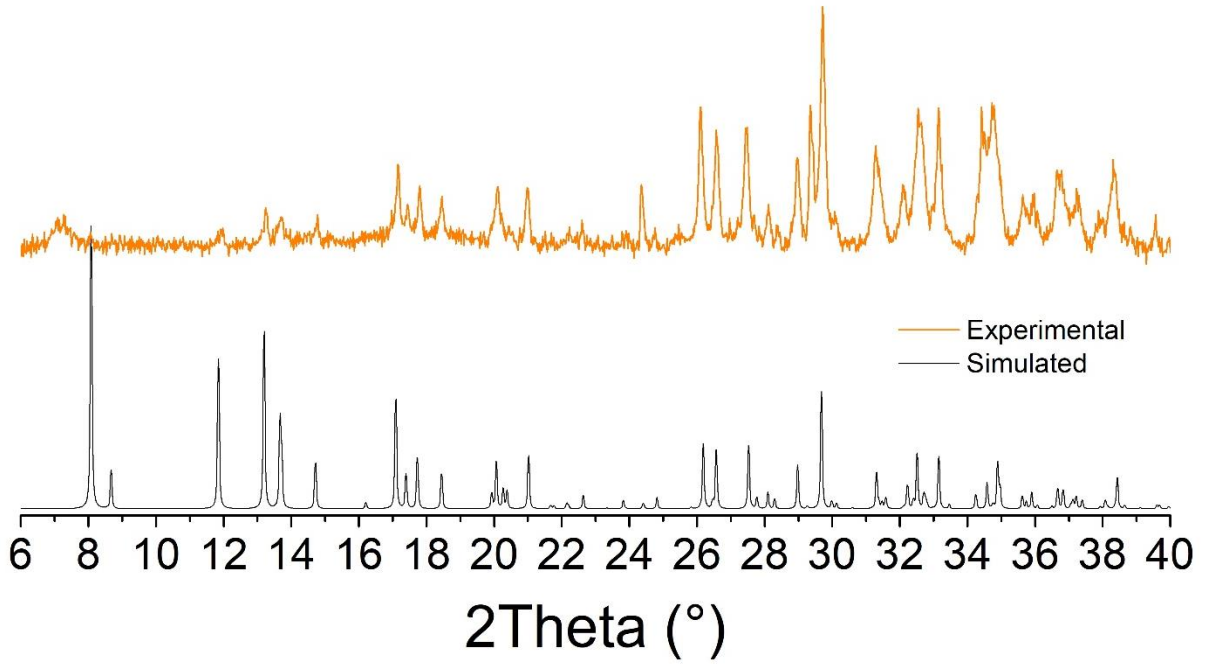

Fig. S11 Simulated and experimental powder X-ray diffraction pattern for (DPP-Py)$BiBr_5$.

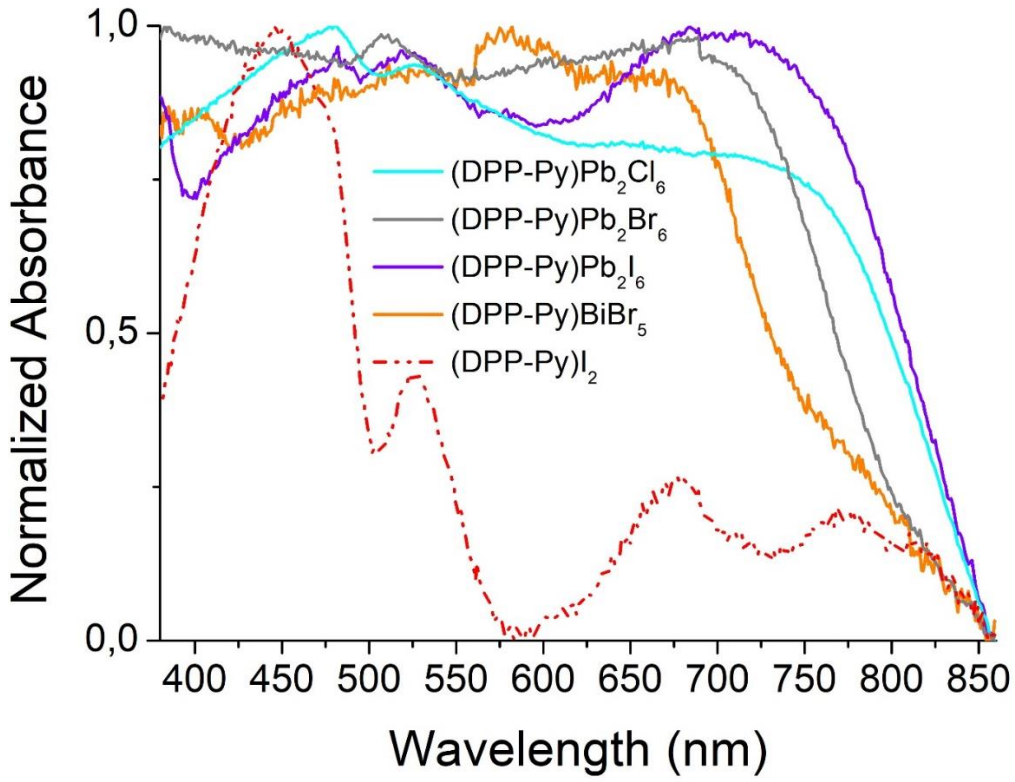

Fig. S12 UV-Vis absorption measurements on pressed pellets of both $(DPP\text{-}Py)I_2$ and hybrid metal-halide compounds.

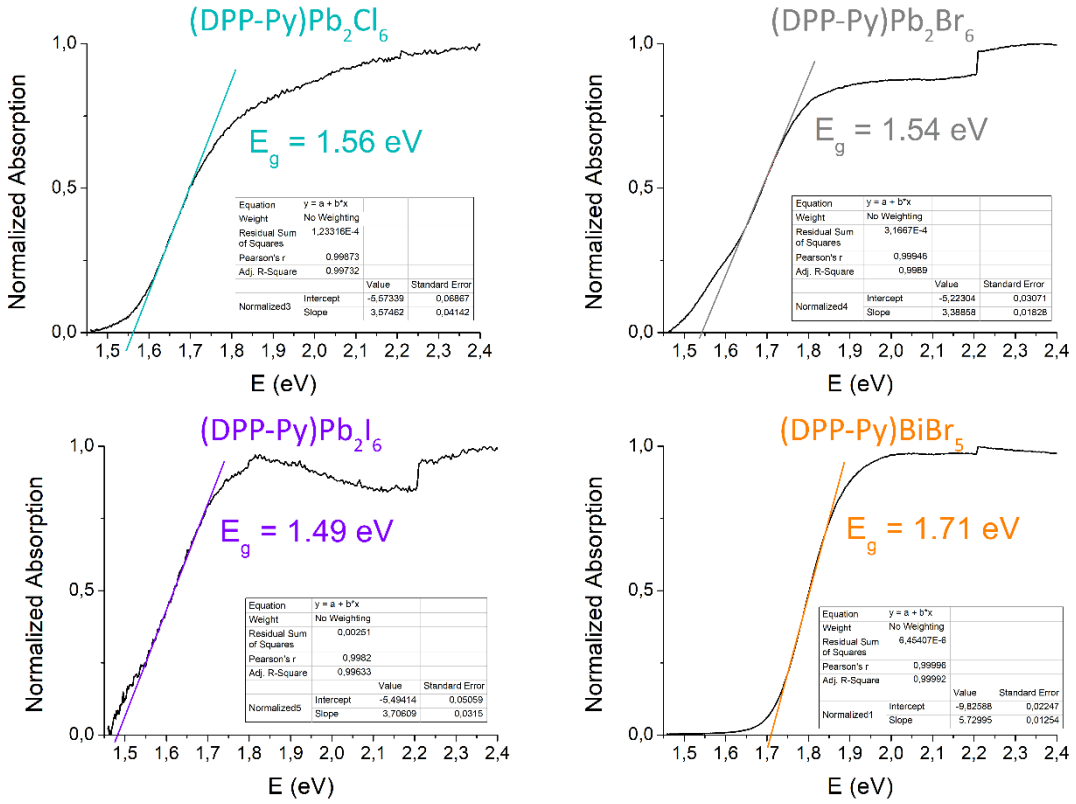

Fig. S13 Optical absorption of the polycrystalline powders obtained from diffuse reflectance measurements converted using the Kubelka-Munk function ($\alpha/S = (1 - R)^2/2R$).

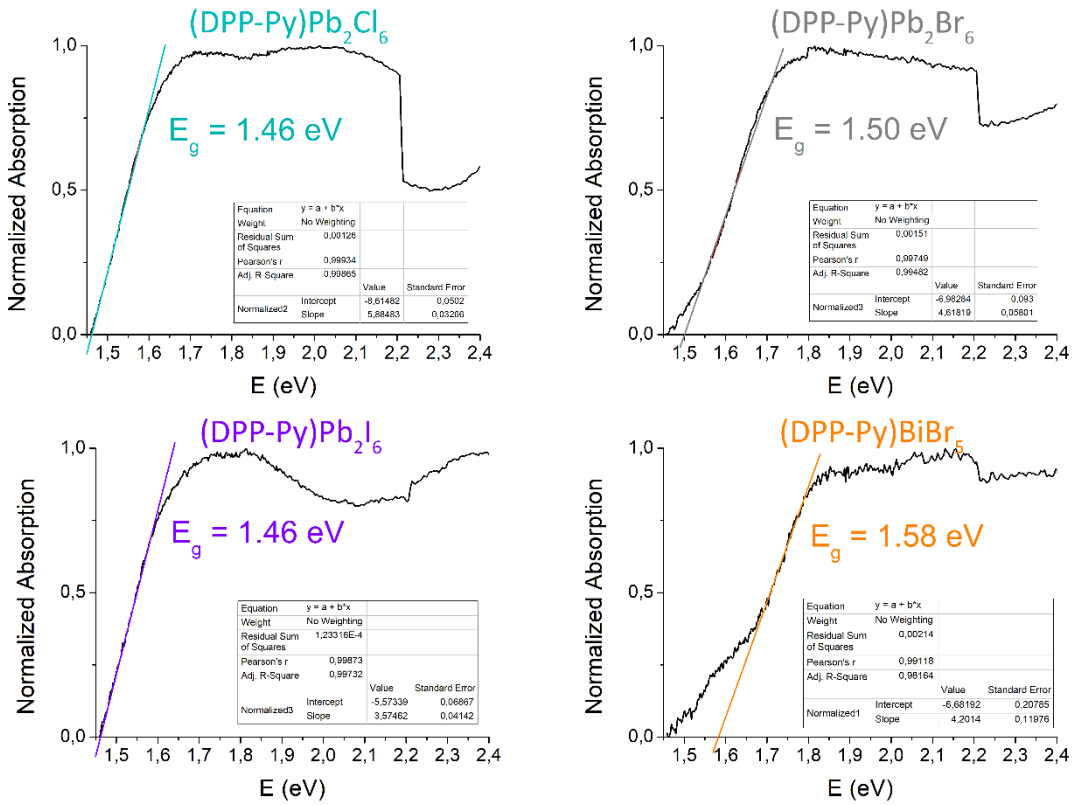

Fig. S14 Optical absorption of the pressed pellets obtained from diffuse reflectance measurements converted using the Kubelka-Munk function ($\alpha/S = (1 - R)^2/2R$).

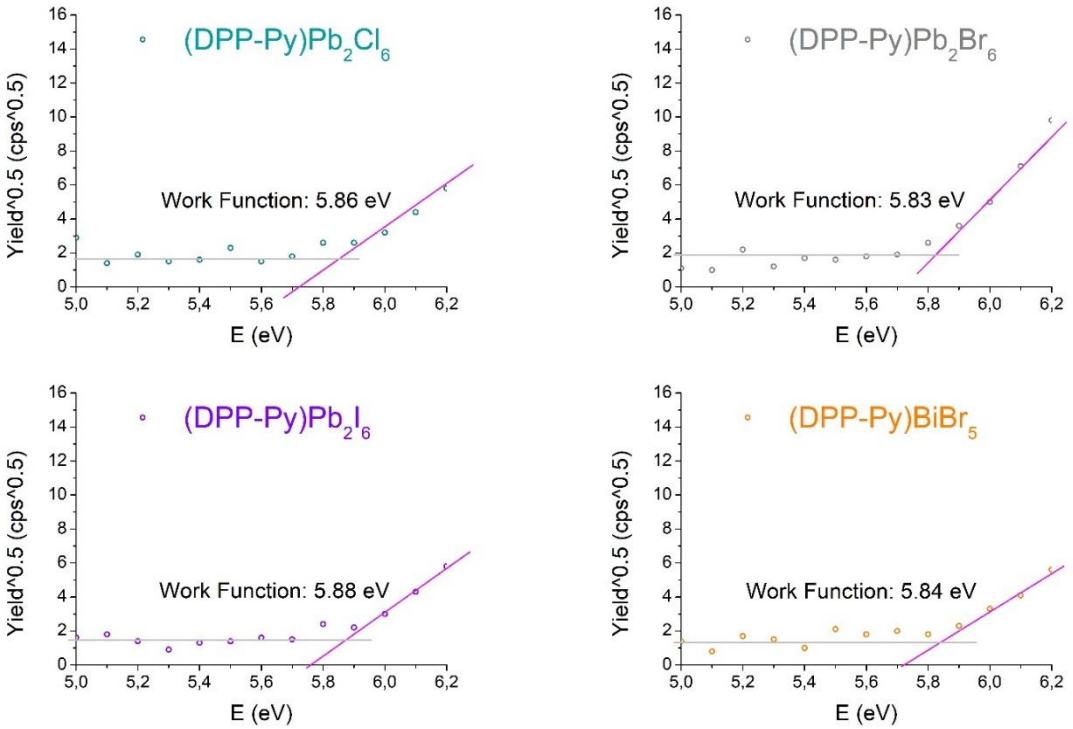

Fig. S15 Photoelectron spectroscopy in air (PESA) measurements of the pressed pellets with linear fittings. The work function is obtained at the intersection between linear fits.

Computational details

First-principles calculations are based on density functional theory (DFT) as implemented in the SIESTA package.[3,4] The non-local van der Waals density functional of Dion *et al.* corrected by Cooper (C09) is used for geometry optimizations[5,6]. Spin-orbit coupling is taken into account through the off-site approach in the Hemstreet formalism.[7] To prevent conflicts between the treatment of spin-orbit coupling and the nonlocality of C09, single point calculations are conducted with the revPBE functional.[8] Core electrons are described with Troullier-Martins pseudopotentials,[9] while valence wavefunctions are developed over double-ζ polarized basis set of finite-range numerical pseudoatomic orbitals.[10] In all cases, an energy cutoff of 150 Ry for real-space mesh size has been used. The Brillouin zones of the primitive cells of (DPP-Py)Pb_2Cl_6, (DPP-Py)Pb_2Br_6, (DPP-Py)Pb_2I_6·DMF, and (DPP-Py)Bi_2Br_5, are sampled using 7×3×3, 7×3×3, 5×5×1, and 5×5×7 G-centered Monkhorst-Pack grid, respectively. Experimental structures are used for the inorganic skeleton, well characterized by X-ray diffraction. As this is not the case for light atoms, the positions of organic cations have been optimized until forces are lower than 0.01 eV/Å.

To overcome the shortcomings of plain DFT, we correct the band gap using the hybrid functional PBE0.[11,12] Hybrid functionals are not available in the current implementation of SIESTA, hence, we carry single point calculations using the VASP package[13,14] with reduced k-point sampling (2×2×2 for (DPP-Py)Pb_2Cl_6, (DPP-Py)Pb_2Br_6, and (DPP-Py)Bi_2Br_5, 2×2×1 for (DPP-Py)Pb_2I_6·DMF), and both GGA and PBE0 functionals. The correction obtained from the hybrid functional $D^{hyb} = E_G^{PBE0} - E_G^{GGA}$ is then reported on the band gaps obtained by SIESTA calculations (Table S3). The band structures featured Fig. 5 are obtained by shifting the conduction bands to match the corrected band gap.

---

[3] J. M. Soler, E. Artacho, J. D. Gale, A. García, J. Junquera, P. Ordejón, and D. Sánchez-Portal, *J. Phys.: Condens. Matter* **2002**, *14*, 2745-2779.

[4] A. García, N. Papior, A. Akhtar, E. Artacho, V. Blum, E. Bosoni, P. Brandimarte, M. Brandbyge, J. I. Cerdá, F. Corsetti, R. Cuadrado, V. Dikan, J. Ferrer, J. Gale, P. García-Fernández, V. M. García-Suárez, S. García, G. Huhs, S. Illera, R. Korytár, P. Koval, I. Lebedeva, L. Lin, P. López-Tarifa, S. G. Mayo, S. Mohr, P. Ordejón, A. Postnikov, Y. Pouillon, M. Pruneda, R. Robles, D. Sánchez-Portal, J. M. Soler, R. Ullah, V. W. Yu, and J. Junquera, *J. Chem. Phys.* **2020**, *152*, 204108.

[5] M. Dion, H. Rydberg, E. Schröder, D. C. Langreth, and B. I. Lundqvist, *Phys. Rev. Lett.* **2004**, *92*, 246401.

[6] V. R. Cooper, *Phys. Rev. B: Condens. Matter Mater. Phys.* **2010**, *81*, 161104.

[7] R. Cuadrado, and J. I. Cerdá, *J. Phys.: Condens. Matter* **2012**, *24*, 086005.

[8] Y. Zhang, and W. Yang, *Phys. Rev. Lett.* **1998**, *80*, 890.

[9] N. Trouiller, and J. L. Martins, *Phys. Rev. B* **1991**, *43*, 1993-2006.

[10] E. Artacho, D. Sánchez-Portal, P. Ordejón, A. García, and J. M. Soler, *Phys. Stat. Sol. (b)* **1999**, *215*, 809-817.

[11] J. P. Perdew, M. Ernzerhof, and K. Burke, *J. Chem. Phys.* **1996**, *105*, 9982-9985.

[12] C. Adamo, and V. Barone, *J. Chem. Phys.* **1999**, *110*, 6158-6170.

[13] G. Kresse, and J. Furthmüller, Comput. Mat. Sci. **1996**, *6*, 15-50.

[14] G. Kresse, Phys. Rev. B **1996**, *54*, 11169-11186.

Finally, complementary molecular calculations on the DPP-Py^{2+} cation are performed using Gaussian16,[15] with the PBE0 functional and the 6-31+G* basis sets. Excited-state properties are explored using time-dependent DFT (TD-DFT), considering 20 excited states. The energy difference between the lowest unoccupied molecular orbital (LUMO) and the highest occupied molecular orbital (HOMO) is larger than the energy of the first excited state with non-zero oscillator strength. We label this difference $D^{TD\text{-}DFT}$. In the case of DPP-Py^{2+}, we find $D^{TD\text{-}DFT}$ = –0.272 eV.

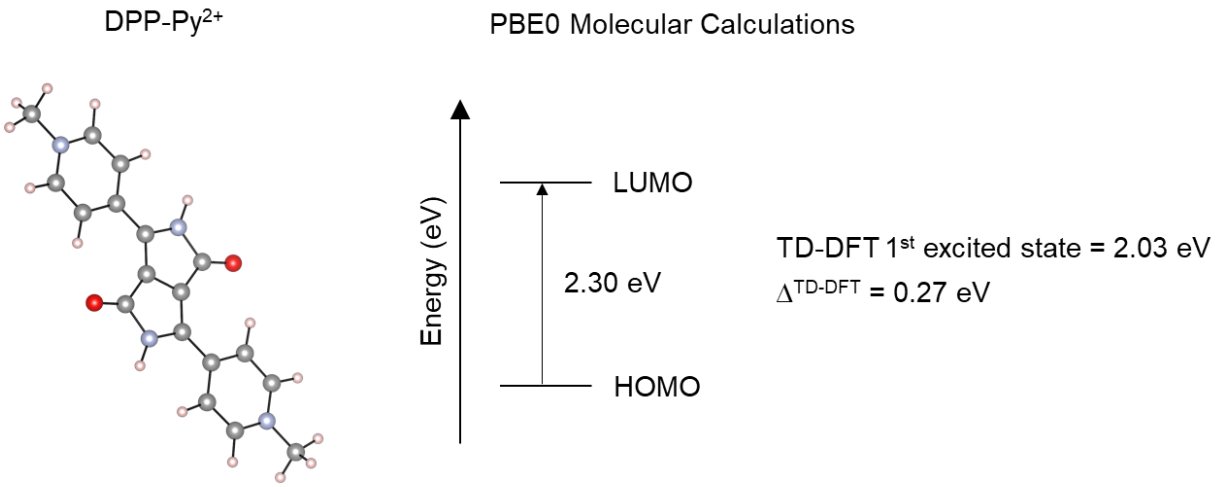

Fig. S16 DFT description of the DPP-Py^{2+} cation. PBE0 molecular calculations computed partial charge density taken at the VBM of (DPP-Py)Pb_2Cl_6, (DPP-Py)Pb_2Br_6, (DPP-Py)Pb_2I_6·DMF, and (DPP-Py)$BiBr_5$. The VBM of (DPP-Py)Pb_2Cl_6 and (DPP-Py)Pb_2Br_6 are distributed over the organic cations, while the VBM of (DPP-Py)Pb_2I_6·DMF and (DPP-Py)$BiBr_5$ involve the inorganic network.

[15] Gaussian 16, Revision C.01, M. J. Frisch, G. W. Trucks, H. B. Schlegel, G. E. Scuseria, M. A. Robb, J. R. Cheeseman, G. Scalmani, V. Barone, G. A. Petersson, H. Nakatsuji, X. Li, M. Caricato, A. V. Marenich, J. Bloino, B. G. Janesko, R. Gomperts, B. Mennucci, H. P. Hratchian, J. V. Ortiz, A. F. Izmaylov, J. L. Sonnenberg, D. Williams-Young, F. Ding, F. Lipparini, F. Egidi, J. Goings, B. Peng, A. Petrone, T. Henderson, D. Ranasinghe, V. G. Zakrzewski, J. Gao, N. Rega, G. Zheng, W. Liang, M. Hada, M. Ehara, K. Toyota, R. Fukuda, J. Hasegawa, M. Ishida, T. Nakajima, Y. Honda, O. Kitao, H. Nakai, T. Vreven, K. Throssell, J. A. Montgomery, Jr., J. E. Peralta, F. Ogliaro, M. J. Bearpark, J. J. Heyd, E. N. Brothers, K. N. Kudin, V. N. Staroverov, T. A. Keith, R. Kobayashi, J. Normand, K. Raghavachari, A. P. Rendell, J. C. Burant, S. S. Iyengar, J. Tomasi, M. Cossi, J. M. Millam, M. Klene, C. Adamo, R. Cammi, J. W. Ochterski, R. L. Martin, K. Morokuma, O. Farkas, J. B. Foresman, and D. J. Fox, Gaussian, Inc., Wallingford CT, 2016.

Table S3 Experimental and computed band gaps and band gap corrections (eV), using GGA and the PBE0 hybrid functional with VASP, the GGA functional with SIESTA. The PBE0-based TD-DFT calculation run on DPP-Py^{2+} with Gaussian16 provides an additional correction of $D^{TD\text{-}DFT}$ = – 0.272 eV between the electronic and optical gap of organic cation.

	(DPP-Py)Pb_2Cl_6	**(DPP-Py)Pb_2Br_6**	**(DPP-Py) Pb_2I_6·DMF**	**(DPP-Py)Bi_2Br_5**
Exp. Optical Gap	1.56	1.54	1.49	1.71
VASP GGA	0.726	0.733	0.661	0.829
VASP PBE0	1.881	1.892	2.061	2.156
Δ^{hyb}	1.155	1.159	1.400	1.327
SIESTA GGA	0.735	0.747	0.477	0.806
SIESTA GGA+Δ^{hyb}	1.890	1.906	1.877	2.133
SIESTA GGA+Δ^{hyb}+$\Delta^{TD\text{-}DFT}$	1.618	1.634	1.605	1.861

Table S4 GGA computed effective masses (m_0) for (DPP-Py)Pb_2Cl_6, (DPP-Py)Pb_2Br_6, (DPP-Py)Pb_2I_6·DMF, and (DPP-Py)Bi_2Br_5.

	VBM			**CBM**		
	a	**b**	**c**	**a**	**b**	**c**
(DPP-Py)Pb_2Cl_6	-0.482	-1.789	-1.619	7.584	0.953	0.908
(DPP-Py)Pb_2Br_6	-0.625	-3.184	-1.130	29.77	1.100	1.347
(DPP-Py) Pb_2I_6·DMF	-23.44	-5.758	-0.833	1.412	3.177	3.177
(DPP-Py)Bi_2Br_5	-3.029	-0.300	-2.046	-58.70	0.507	1.023

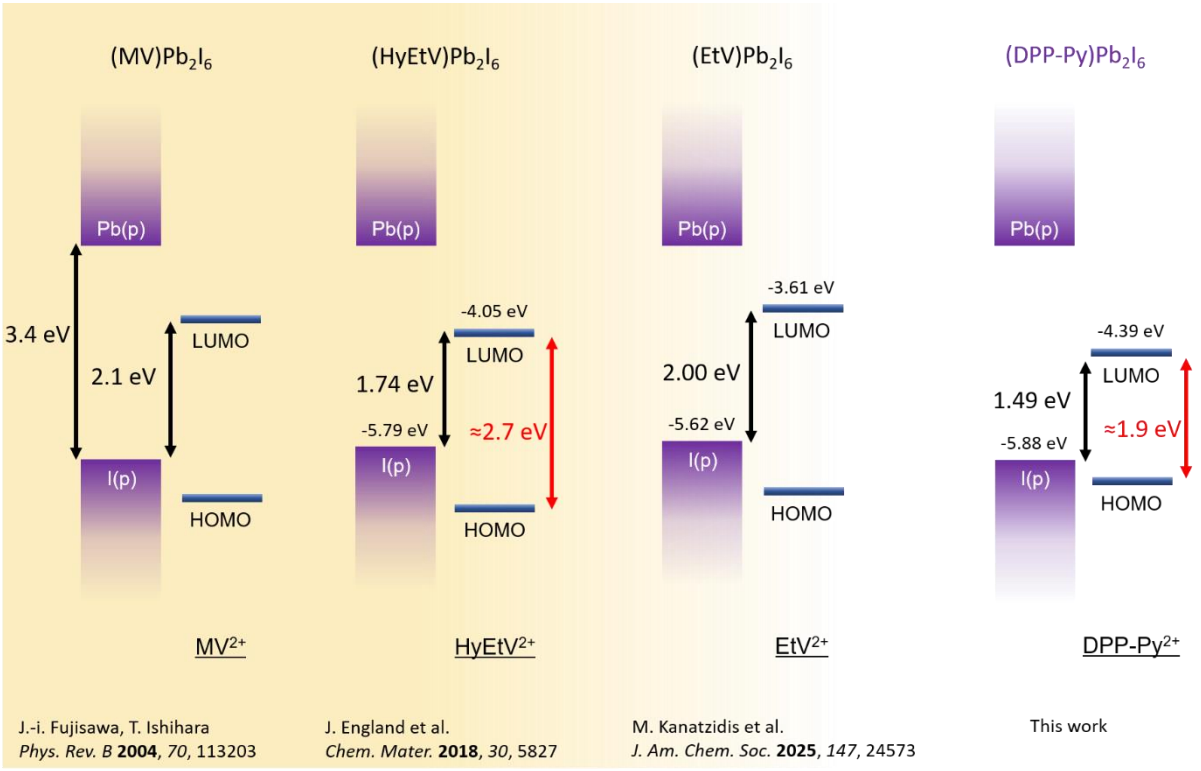

Fig. S17 Comparison between schematic energy diagrams for the previously reported compounds $(MV)Pb_2I_6$, $(HyEtV)Pb_2I_6$ and $(EtV)Pb_2I_6$, and for the new compound $(DPP\text{-}Py)Pb_2I_6$.

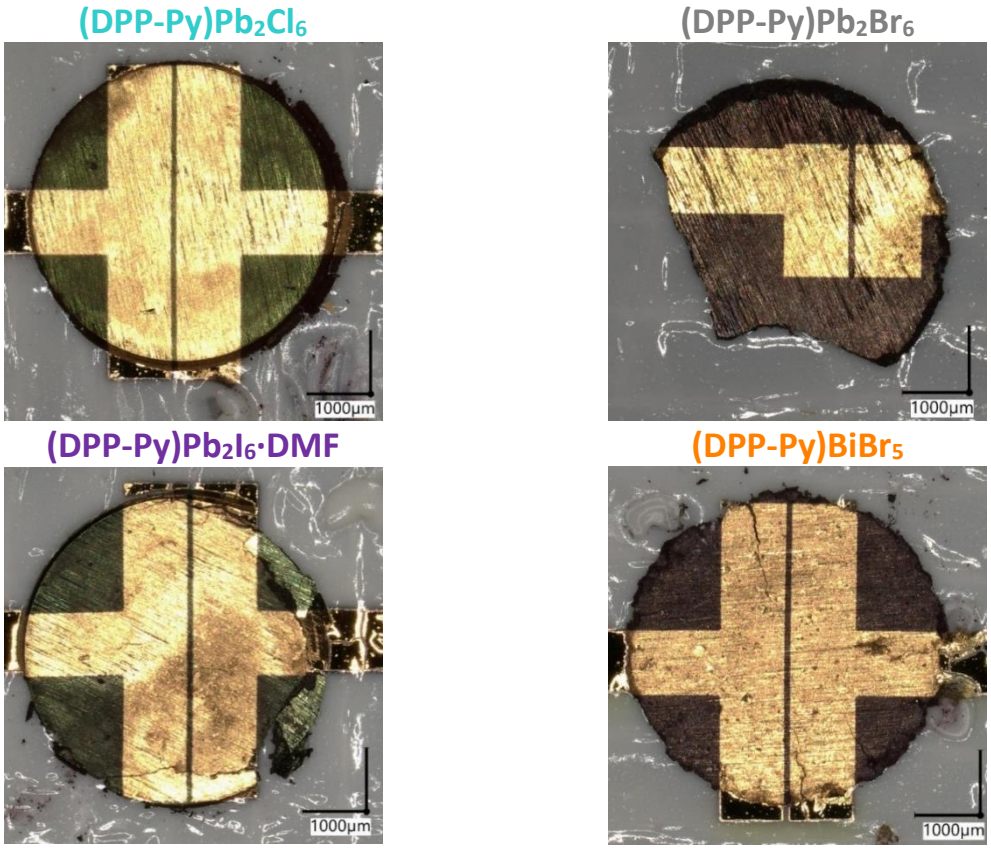

Fig. S18 Pictures of the gold contacts deposited on the pressed pellets of $(DPP\text{-}Py)Pb_2Cl_6$, $(DPP\text{-}Py)Pb_2Br_6$, $(DPP\text{-}Py)Pb_2I_6{\cdot}DMF$ and $(DPP\text{-}Py)BiBr_5$.

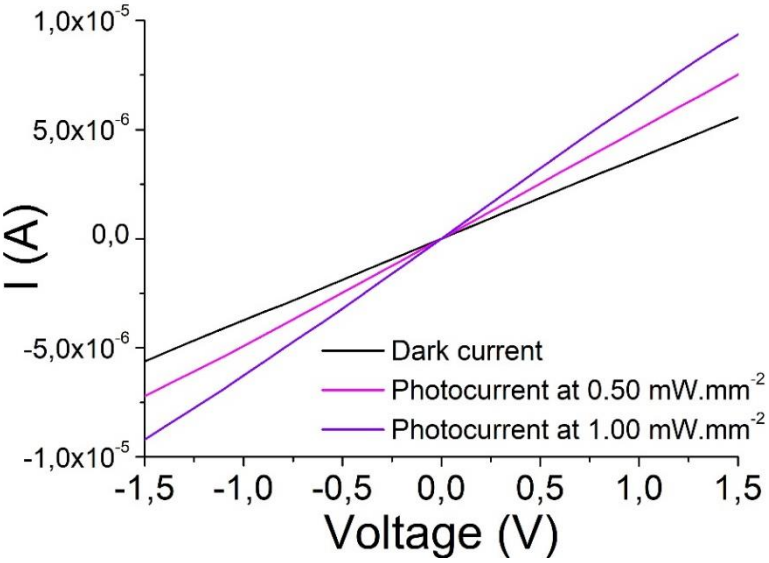

Fig. S19 I-V characteristics of (DPP-Py)Pb_2I_6·$(DMF)_2$.

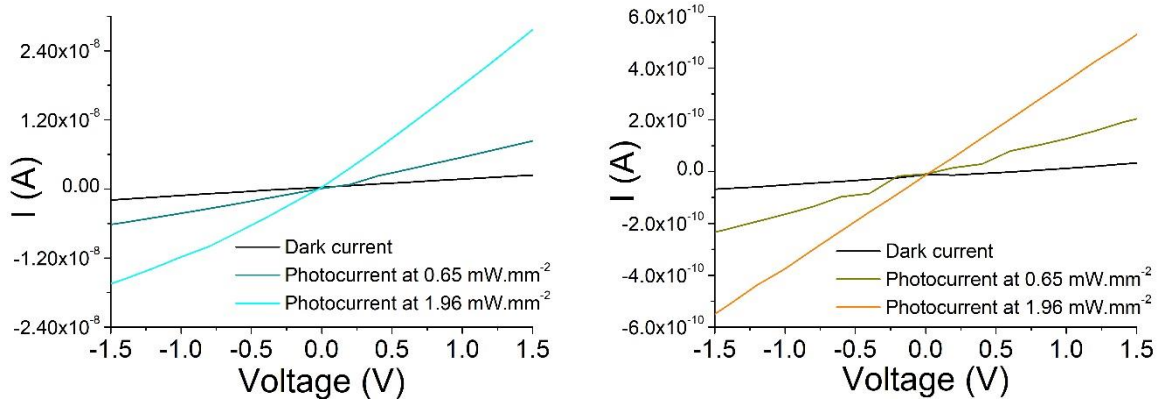

Fig. S20. I-V characteristics of (DPP-Py)Pb_2Cl_6 (left) and (DPP-Py)$BiBr_5$ (right) seven months and nine month, respectively, after the first series of measurements reported in the main text.

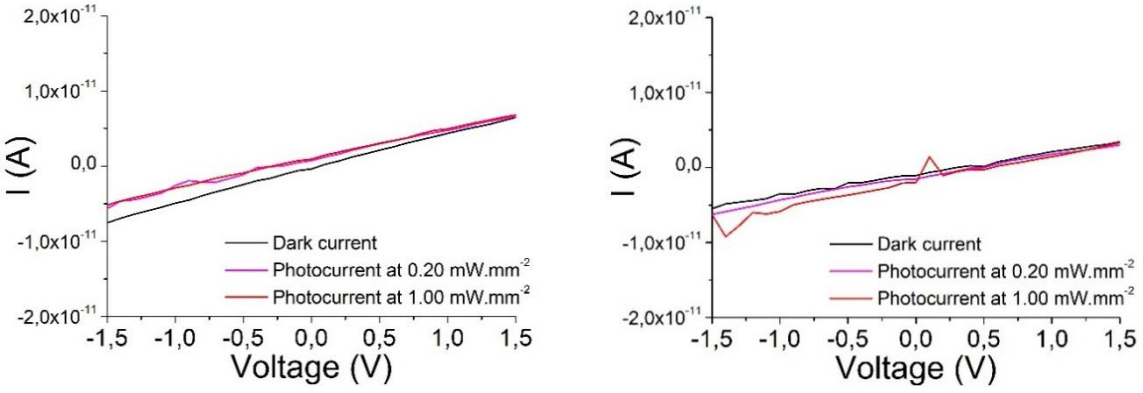

Fig. S21 I-V characteristics on two different pellets of (DPP-Py)I_2.